

UCLA

UCLA Previously Published Works

Title

Structure of *S. pombe* telomerase protein Pof8 C-terminal domain is an xRRM conserved among LARP7 proteins

Permalink

<https://escholarship.org/uc/item/9rj7t5v4>

Journal

RNA Biology, 18(8)

ISSN

1547-6286

Authors

Basu, Ritwika
Eichhorn, Catherine D
Cheng, Ryan
[et al.](#)

Publication Date

2021-08-03

DOI

10.1080/15476286.2020.1836891

Peer reviewed

RESEARCH PAPER



Structure of *S. pombe* telomerase protein Pof8 C-terminal domain is an xRRM conserved among LARP7 proteins

Ritwika Basu^{*,#}, Catherine D. Eichhorn^{*,&}, Ryan Cheng, Robert D. Peterson, and Juli Feigon

Department of Chemistry and Biochemistry, University of California, Los Angeles, CA, USA

ABSTRACT

La-related proteins 7 (LARP7) are a class of RNA chaperones that bind the 3' ends of RNA and are constitutively associated with their specific target RNAs. In metazoa, Lar7 binds to the long non-coding 7SK RNA as a core component of the 7SK RNP, a major regulator of eukaryotic transcription. In the ciliate *Tetrahymena* the LARP7 protein p65 is a component of telomerase, an essential ribonucleoprotein complex that maintains the telomeric DNA at eukaryotic chromosome ends. p65 is important for the ordered assembly of telomerase RNA (TER) with telomerase reverse transcriptase. Unexpectedly, *Schizosaccharomyces pombe* Pof8 was recently identified as a LARP7 protein and a core component of fission yeast telomerase essential for biogenesis. LARP7 proteins have a conserved N-terminal La motif and RRM1 (La module) and C-terminal RRM2 with specific RNA substrate recognition attributed to RRM2, first structurally characterized in p65 as an atypical RRM named xRRM. Here we present the X-ray crystal structure and NMR studies of *S. pombe* Pof8 RRM2. Sequence and structure comparison of Pof8 RRM2 to p65 and human Lar7 xRRMs reveals conserved features for RNA binding with the main variability in the length of the non-canonical helix α 3. This study shows that Pof8 has conserved xRRM features, providing insight into TER recognition and the defining characteristics of the xRRM.

ARTICLE HISTORY

Received 22 August 2019
Revised 6 October 2020
Accepted 11 October 2020

KEYWORDS

La protein; LARP; RRM; NMR; X-ray crystallography; telomerase; xRRM; RNA; 7SK



Introduction

The eukaryotic La protein and La-related protein (LARP) superfamily bind to diverse RNA targets and are involved in RNA processing and assembly [1–3]. Genuine La protein recognizes the 3' UUU-OH terminus of most nascent RNA polymerase III transcripts to protect and stabilize them and in many cases also acts as a chaperone to fold the RNAs into functional complexes [4–10].LARPs bind to specific RNAs to function in the folding and biogenesis of their ribonucleoproteins (RNPs) [2]. Based on evolutionary and domain organization conservation, they have been classified into four families (LARP1, LARP4, LARP6 and LARP7), and the LARP7 family appears most closely related to genuine La protein [1–3].

All LARP7 proteins identified to date are components of 7SK [11,12] or telomerase RNPs [13–17]. The 7SK RNP sequesters and inactivates the kinase activity of the positive transcription elongation factor b (P-TEFb) to regulate the elongation phase of RNA Polymerase II [18,19] and has been identified in metazoa [20,21]. Lar7 (here lowercase is used to distinguish the protein name in metazoa from the LARP7 family) binds to the long-noncoding 7SK RNA as a core component of the 7SK RNP and is required for 7SK RNP hierarchical assembly with P-TEFb and transcription regulation [11,12,22,23]. Telomerase is an RNP that maintains

telomeric DNA repeats at the ends of linear chromosomes [24,25] and has been identified in most eukaryotes [26,27]. Telomerase is comprised of the telomerase RNA (TER) scaffold and template and the telomerase reverse transcriptase (TERT) enzyme, required together for catalytic activity, and additional proteins required for biogenesis and activity that form the holoenzyme *in vivo* [26,28,29]. In the ciliates *Tetrahymena thermophila* and *Euplotes aediculatus*, the respective LARP7 protein p65 and p43 binds to TER and is required for its assembly with TERT [13,14,30–32]. Recently, a LARP7 protein, Pof8 (also called Lar7), was identified in the fission yeast *Schizosaccharomyces pombe* [15–17]. Pof8 binds to the *S. pombe* telomerase RNA (TER1) and recruits TER1 processing proteins Lsm2-8 to facilitate assembly of TER1 with TERT, and is essential for telomerase biogenesis and function [15–17].


LARP7s have three structured domains – an N-terminal-winged helix domain (La motif, LaM) followed by an RNA recognition motif (RRM1) that together form a La module, and a C-terminal atypical RRM2 [2] (Fig. 1A). The La module is a conserved feature of genuine La and LARPs that specifically recognizes and binds to the RNA 3' UUU-OH end [4,5,7], although the genuine La protein and LARP6 La modules sometimes bind alternate sequences [9,33,34]. The

CONTACT Juli Feigon  feigon@mbi.ucla.edu  Department of Chemistry and Biochemistry, University of California, Los Angeles, CA, USA

*These authors are contributed equally to this work.

#Current address: Department of Microbiology and Immunology, University of Texas Medical Branch, Galveston, TX 77555

&Current address: Department of Chemistry, University of Nebraska, Lincoln, NE 68508

 Supplemental data for this article can be accessed [here](#).

© 2020 Informa UK Limited, trading as Taylor & Francis Group

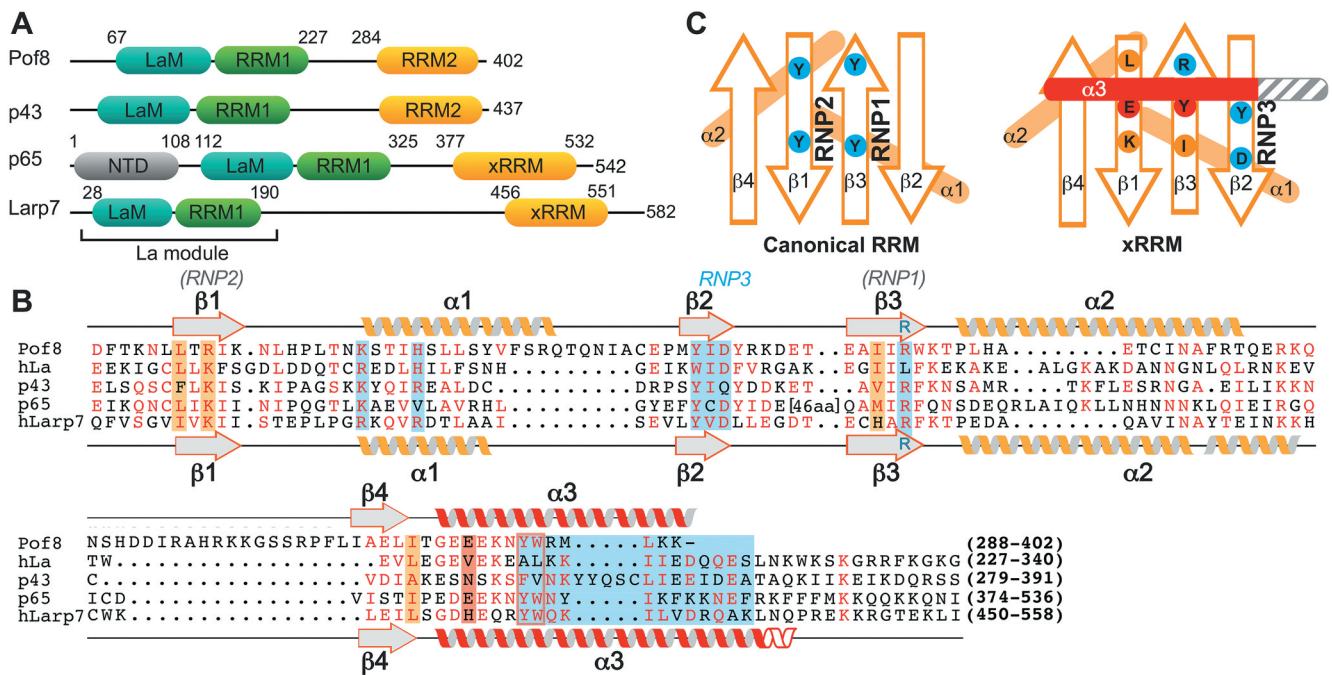


Figure 1. Domains and sequence alignments of LARP7 and La proteins (A) Domain organization of LARP7s from yeast *S. pombe* (Pof8), ciliate *Euplotes aediculatus* (p43), ciliate *Tetrahymena thermophila* (p65), and human (Larp7). Numbers above the sequence schematic indicate known domain boundaries of the La motif (cyan), RRM1 (green) and xRRM (orange). (B) Sequence alignment of LARP7 p65 and Larp7 xRRMs, human La protein (hLa) RRM2, Pof8, and *Euplotes* p43. Residues with high similarity are coloured red. The secondary structure elements of Pof8 and hLarp7 are shown as helices and sheets above and below the sequence, respectively. Locations of RNP1 and RNP2 in canonical RRM are indicated above the sequence in brackets for reference. Conserved residues determined by this and previous work to contribute to RNA binding and helix α 3- β sheet interaction are sky blue and orange (for β -sheet) and red (for α 3), respectively. (C) Cartoon comparing the conserved RNA binding features of a canonical RRM (left) and xRRM (right), based in part on this work. Conserved residues that bind RNA are shown in sky blue and that contribute to the helix α 3- β sheet interaction are shown in red and orange, respectively. For the canonical RRM, circled residues are those that most commonly interact with RNA. For the xRRM, the length of helix α 3 (shown in grey) varies. Variable regions not involved in RNA binding (β 4' strand and loops) not pictured.

La module of ciliate and metazoan LARP7s binds to the 3' UUU-OH terminus of their TER and 7SK cognate RNAs, respectively [23,35,36]. For both *Tetrahymena* p65 and human Larp7, the C-terminal RRM2 is essential for specific RNA recognition and RNP assembly [22,31,32,37]. High-resolution structures of these domains in complex with RNA revealed an atypical mode of RNA binding divergent from that of canonical RRM [38-40], and the domain was named xRRM for extended helical RRM [31,41,42]. Compared to the canonical RRM, the xRRM lacks conserved single-strand RNA recognition sequences RNP1 (K/R-G-F/Y-G/A-F/Y-I/L/V-X-F/Y) and RNP2 (I/L/V-F/Y-I/L/V-X/N/L) on the β -sheet and has an additional C-terminal helix α 3 that lies across this surface (Fig. 1B,C) [40,41]. These structures, together with multiple sequence alignment of LARP7s with predicted xRRMs, revealed several conserved features key for RNA recognition: a Y/W-X-D/Q (RNP3) sequence on strand β 2 (where underline indicates residues that interact with RNA), a conserved R on strand β 3, and charged/aromatic residues on the C-terminal end of helix α 3 (Fig. 1B, C) that together form an RNA binding surface on the side of the β -sheet rather than the surface and recognize a combination of base paired and unpaired nucleotides with high affinity and specificity [31,41,42]. *Euplotes* LARP7 telomerase protein p43, a homolog of p65, binds a similar site in TER as p65 [13,30,43]. Based on sequence and homology modelling it is predicted to contain an xRRM

[31,42]. Human genuine La contains an atypical RRM with most of the features of an xRRM (Fig. 1B) and has chaperone activity [44,45], but the RNA-binding mode remains unknown.

The fission yeast LARP7 protein Pof8 was predicted to contain an xRRM at its C-terminus based on sequence similarity to *Tetrahymena* p65 and human Larp7 [15-17]. Loss of Pof8 severely reduces telomerase activity *in vivo* and results in critically short telomeres, ultimately leading to uncapped chromosomes and chromosome end fusions [16]. Truncation constructs deleting the putative RRM2 domain reduced TER1-TERT assembly, TER1 levels, and had a similar phenotype to Pof8 knock-down [16]. Previously, association of a LARP7 protein with telomerase RNA was thought to be unique to ciliates, whose TER is an RNA polymerase III transcript with a native 3' UUU-OH terminus that binds the La module. Although this 3'-end sequence is absent in RNA polymerase II mRNA transcripts, the intron-encoded fission yeast TER1 is spliced resulting in a 3' UUU-OH terminus [46,47]. However, the Lsm2-8 proteins bind to this region [48], ostensibly preventing La module interaction with the 3' terminus. The complete secondary structure of the 1213 nt TER1 has not been established and the binding site(s) for Pof8 is unknown. Although less well characterized, there is evidence that hLarp7 plays a role in human telomerase abundance and activity [49], suggesting that LARP7s may be broadly involved in telomerase function.

Here we present a 1.35 Å resolution crystal structure and solution NMR study of the C-terminal domain of Pof8, which reveals features consistent with an xRRM, despite having a shorter helix α 3. We compare the structure with p65 and hLarp7 xRRM structures in the absence and presence of their cognate RNAs [31,42,50], as well as with genuine La RRM2 [44], to refine the sequence and structural features of the xRRM class of atypical RRMs, and we propose the RNA binding mode in Pof8.

Results

Crystal structure of the Pof8 C-terminal domain

Based on sequence homology and predicted secondary structure, a La module and RRM2 were predicted at Pof8 N- and C-termini, respectively [15–17] (Fig. 1A). In particular, the C-terminal RRM2 domain has significant sequence homology to the xRRM domains in *Tetrahymena* p65 [31] and human Larp7 [50] (Fig. 1B). Based on sequence alignment and known RRM topology (Fig. 1C), a Pof8 construct containing residues 282–402 was cloned into a pET vector containing an N-terminal His₆-SUMO fusion protein, and recombinant protein was expressed, purified, and screened by solution NMR spectroscopy to identify the presence of a folded domain. The Pof8 construct was crystallized, with crystals diffracting to 1.35 Å in space group P3121 (Table 1). The structure was determined by heavy atom (Hg) phasing using PCMBS-soaked crystals. The electron density of the protein was visible up to 2 σ , with weak density for residues 376–378 and no

density was observed for N-terminal residues 282–287 or C-terminal residue 402 (Fig. 2A). The crystal structure of Pof8 C-terminal domain revealed an atypical RRM with an overall β 1- α 1- β 2- β 3- α 2- β 4- α 3 topology. A four-stranded anti-parallel β -sheet consisting of β 4 (aa 384–387), β 1 (aa 294–298), β 3 (aa 339–344) and β 2 (aa 329–332) forms the front face with helices α 1 (aa 306–320) and α 2 (aa 347–359) packed on the back of the β -sheet to form the hydrophobic core and helix α 3 (aa 391–401) on top of the β -sheet (Fig. 2B, C). There are four loops: β 1- α 1 (aa 299–305), α 1- β 2 (aa 321–328), β 2- β 3 (aa 333–338), β 3- α 2 (aa 345–346), α 2- β 4 (aa 360–383), and β 4- α 3 (aa 388–390). Helix α 3 (not present in canonical RRMs) is positioned orthogonal to the long axis of the β -strands, and lies across where the canonical RNP1 and RNP2 residues are normally found. Canonical RNP1 and RNP2 sequences on β 3 and β 1, respectively, are absent and there is a Y330–I331–D332 sequence on β 2 (RNP3) and R343 on β 3, consistent with an xRRM (Figs. 1C, 2D) [41].

The Pof8 RRM2 helix α 3 has three turns and is positioned through electrostatic and hydrophobic interactions with the β -sheet and the N-terminal residues (aa 289–294) (Fig. 2E,F). There is a salt bridge between R296 (β 1) and E392 (α 3) side-chains, a hydrogen bond between the N292 backbone amide (N-tail) and the E393 side-chain (α 3), and a hydrogen bond between D332 (β 2) and Y396 (α 3) side-chains. Residues L294 (β 1), I341 (β 3), I388 (β 4- α 3 loop), and Y396 (α 3) form hydrophobic contacts at the β -sheet – helix α 3 interface. The I341 (β 3) side-chain stacks below the aromatic ring of Y396 (α 3), and the W397 (α 3) side-chain has π - π stacking with Y396 (α 3) and F289 (N-tail) side-chains (Fig. 2E,F). Overall, Pof8 RRM2

Table 1. Crystallography statistics for *S. pombe* Pof8 xRRM.

	Native	PCMBS soak
Data Collection		
Wavelength (Å)	0.9791	0.9791
Space Group	P31 2 1	P31 2 1
Cell dimensions a, b, c (Å)	57.36, 57.36, 70.3	56.01, 56.01, 65.29
α , β , γ (°)	90.0, 90.0, 120.0	90.0, 90.0, 120.0
Resolution (Å)	1.35	1.2
R _{merge}	0.044 (0.68)	0.055 (0.5)
R _{measure}	0.049 (0.78)	0.054 (0.58)
R _{pim}	0.022 (0.36)	0.019 (0.17)
I/ σ	16.1 (1.95)	17.1 (3.92)
Completeness (%)	99.1 (98.6)	96.2 (91.0)
No. of total reflections	136156	162043
No. of unique reflections	29661	34507
Multiplicity	4.6 (4.3)	10.0 (9.3)
Wilson B factor	19.47	12.76
CC _{1/2}	0.999 (0.83)	0.998 (0.898)
CC*	1	1
Refinement		
Resolution (Å)	49.67–1.35	48.506–1.2
No. of reflections	29647	69061 (36157)
R _{work} /R _{free}	0.1629/0.1940	0.2216/0.2313
No. of atoms	1019	901
Protein	936	888
Nitrate	4	4
Water	78	13
Average B factors r.m.s.d	17	17
Bond lengths (Å)	0.005	0.007
angles (°)	0.713	0.849
Ramachandran plot		
Favoured (%)	98.23	99.06
Allowed (%)	1.77	0.94
Outliers (%)	0	0

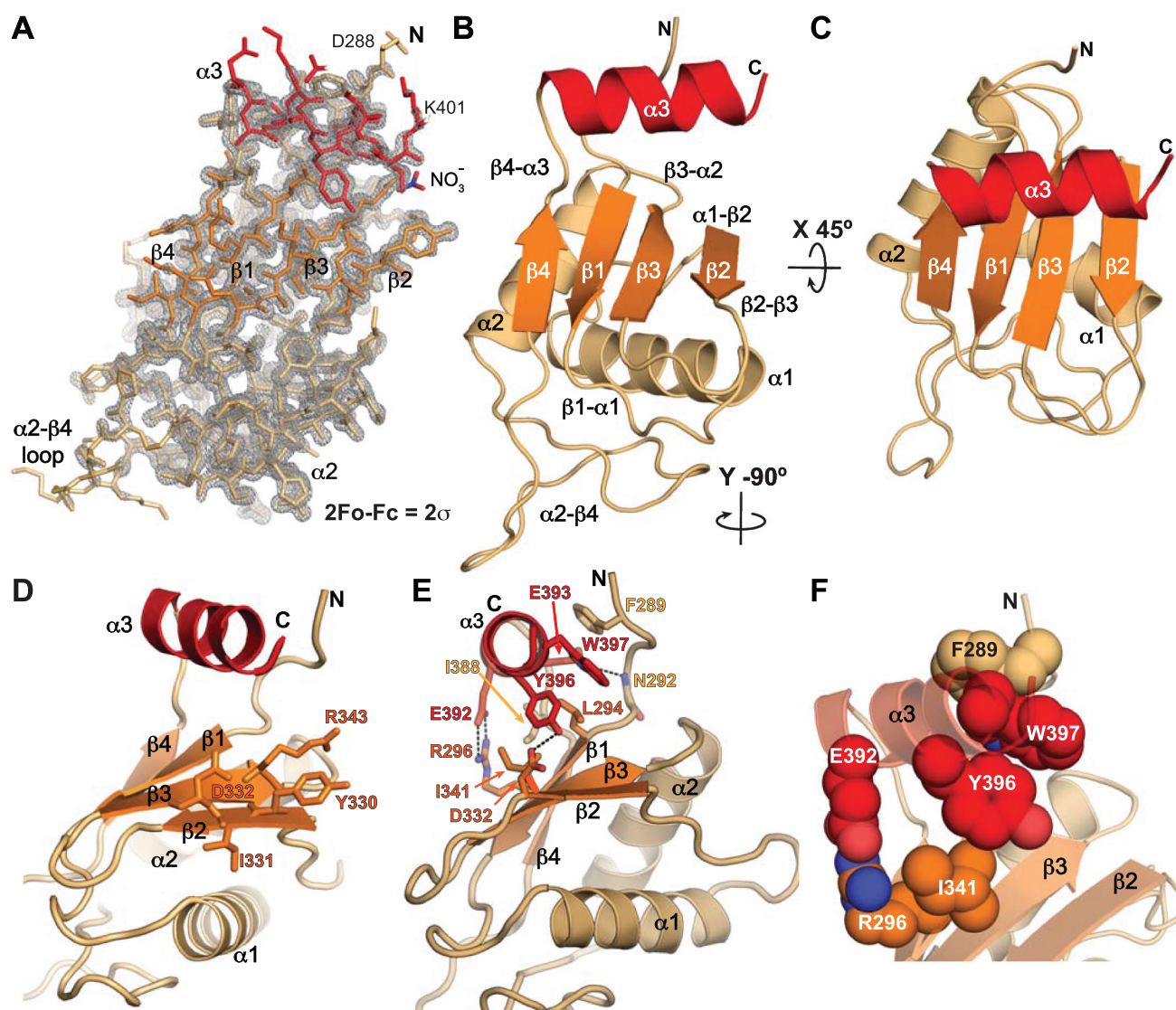


Figure 2. Crystal structure of Pof8 RRM2 at 1.35 Å. (A) 2 Fo-Fc electron density map with crystal structure model shown in stick representation. The map is contoured at 2σ . (B, C) Two views of ribbon representation of the Pof8 xRRM (residues 288–402) crystal structure. The β -sheet is coloured orange, helices $\alpha 1$ and $\alpha 2$ are tan, and helix $\alpha 3$ is red. (D) Ribbon representation with equivalent conserved residues involved in RNA binding in p65 and hLarp7 xRRMs shown as sticks. (E) Ribbon representation with conserved residues involved in stabilizing the $\alpha 3$ - β -sheet interactions shown as sticks. (F) Ribbon representation with conserved residues involved in stabilizing the $\alpha 3$ - β -sheet interactions shown as space fill to highlight stacking interactions.

has all of the characteristic features of an xRRM as previously described except for the absence of residues beyond helix $\alpha 3$ that could extend it upon RNA binding.

Conformational flexibility within the Pof8 RRM2

The global and local dynamics of the Pof8 RRM2 were investigated with solution NMR, using the Pof8 construct used for crystal studies. A 2D ^1H - ^{15}N Heteronuclear Single Quantum Coherence (HSQC) spectrum of the backbone amides shows a well-dispersed set of peaks indicative of a well-folded protein (Fig. 3A). Backbone resonance assignments could be completed for the majority of the Pof8 RRM2, with the exception of $\alpha 2$ - $\beta 4$ loop residues Q350-L383 due to weak peak intensities caused by line broadening, indicative of conformational exchange. Close inspection of the 2D ^1H - ^{15}N HSQC spectrum of the backbone amides revealed

a set of uniformly low-intensity additional peaks that appear to be due to peak doubling, likely caused by a second, lowly populated species in slow exchange with a major species (Fig. 3A,B). 3D resonance assignment confirmed the identities of about half of these peaks. Peak doubling was only observed for the backbone amides. Nearly all of the doubled peaks where the weak peak could be assigned were from residues at the β -sheet – helix $\alpha 3$ interface (T290, N292, K298, E339, I341, E386, E393, W397) or the helix $\alpha 3$ C-terminus (R398, M399, L400, K401) (Fig. 3C). Other weak peaks whose identities could be inferred from proximity to an assigned peak (e.g. L294, T295, R296) also correspond to residues at the β -sheet – helix $\alpha 3$ – N-tail interfaces (Fig. 3A,C).

To determine the conformational flexibility in the major populated conformation of the Pof8 RRM2, we measured ^1H - ^{15}N heteronuclear nuclear Overhauser effects (NOEs) (Fig. 3D). Significantly reduced values are observed for the

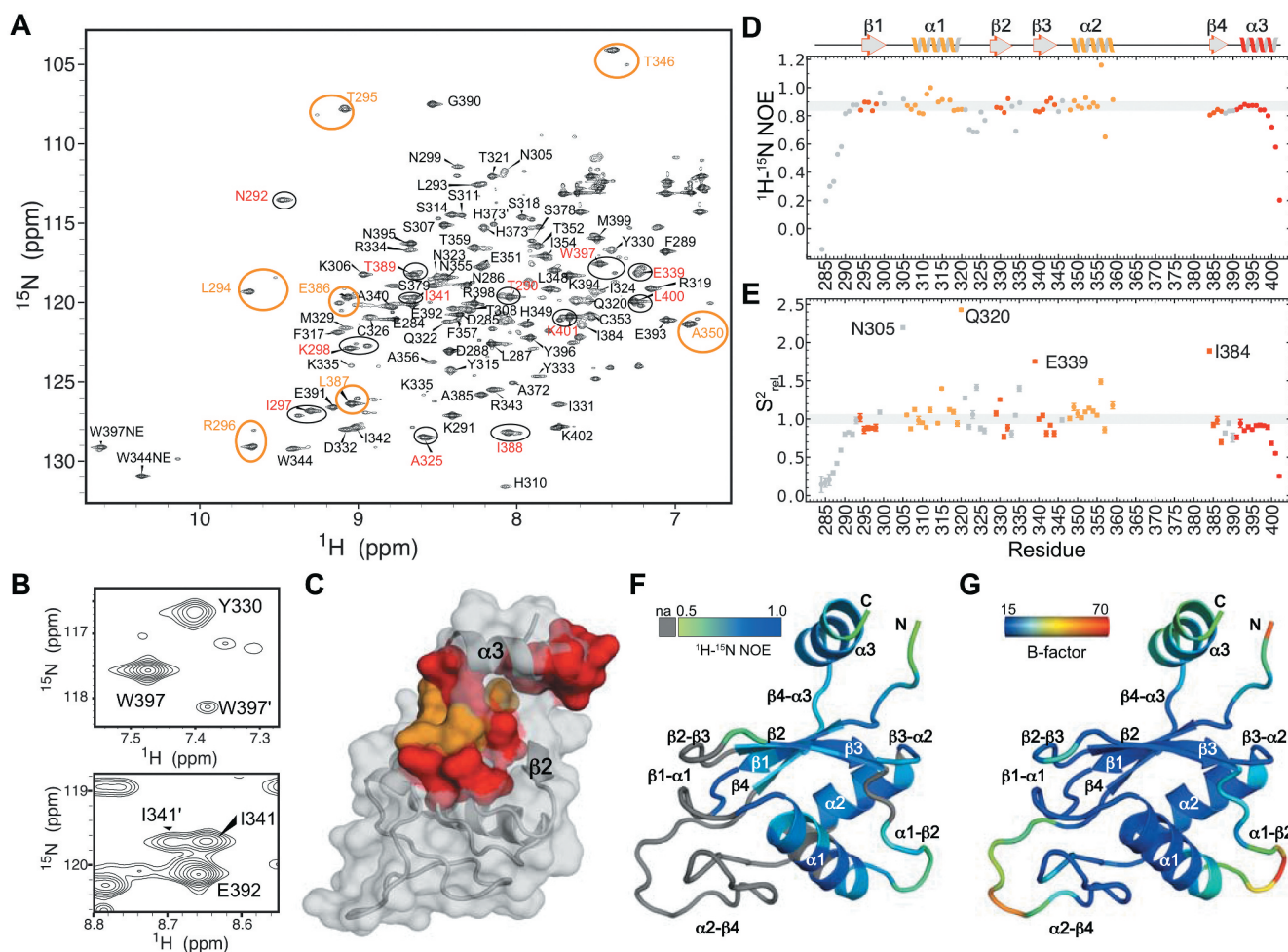


Figure 3. NMR characterization of Pof8 RRM2 (A) ^1H - ^{15}N HSQC spectrum of Pof8 xRRM. Pairs of amide peaks that are doubled are circled; those for which the minor peak is assigned are labelled in red and inferred by proximity to major peak in orange. (B) Expanded regions from panel A showing peak doubling of amides W397 (helix α_3) and I341 (β_3). (C) Distribution of residues whose amides show peak doubling, mapped onto the structure. Assigned residues are red, residues with inferred assignments are orange. (D) Plot of heteronuclear NOE values vs residue number. Secondary structure elements are indicated above. (E) Plot of normalized order parameters vs residue number. Residues with values greater than 1.5 are labelled inset. (F) ^1H - ^{15}N heteronuclear NOE values mapped onto a ribbon structure, with scale ranging from grey (na, not available), 0.5 (green) to 1.0 (blue). (G) Crystal structure B-factor mapped on a ribbon structure, scale ranging from 15.00 (blue) to 70.00 (red).

backbone amides of N-terminal residues E284-F289 and C-terminal residues L400-K402, indicating that the N- and C-termini are highly flexible relative to the globular RRM fold. This data is consistent with the X-ray crystal electron density map that had missing density for N-terminal residues K282 to L287 and C-terminal residue K402. Reduced ^1H - ^{15}N heteronuclear NOE values are also observed for residues Q322-C326 (α_1 - β_2 loop) and residues R334-A340 (β_2 - β_3 loop). To further probe these dynamics, we measured ^{15}N R_1 and R_2 spin relaxation parameters and computed relative order parameters for backbone amide residues [51] (Fig. 3E and Supplemental Table 1). The relative order parameters (S^2_{rel}) describe the relative degree of order with values ranging from zero, representing minimum order, and one, representing maximum order within the molecule. Consistent with ^1H - ^{15}N heteronuclear NOE values, reduced values are observed for N-terminal residues E284-F298 and C-terminal residues L400-K402. However, S^2_{rel} values greater than one were observed for several residues including N305 located at the β_1 - α_1 loop; Y315 and Q320 located on the helix α_1

surface; I324 located in the α_1 - β_2 loop; K335 and E339, located at the β_2 - β_3 loop and β_3 edge; and A356, T359, and I384 adjacent to the α_2 - β_4 loop (Fig. 3E). Inspection of R_1 and R_2 values indicates that the elevated S^2_{rel} values are due to elevated R_2 values, likely due to contributions from chemical exchange between two or more states. Consistent with chemical exchange occurring at these residues, ^1H - ^{15}N heteronuclear NOE, R_1 , and R_2 values could not be measured for the β_1 - α_1 loop, β_2 - β_3 loop, and α_2 - β_4 loop due to extensive line broadening, likely due to chemical exchange (Fig. 3D,E). Consistent with NMR data, the crystallographic B-factors indicate that the hydrophobic core is stable and that the N-terminus, α_1 - β_2 loop, β_2 - β_3 loop, α_2 - β_4 loop, and helix α_3 have higher B-factors (Fig. 3F-G). In addition, although the α_2 - β_4 loop has higher B-factors, there is clear albeit weak electron density for it (Fig. 2A), while these residues could not be assigned due to conformational exchange. We attribute these differences to crystal contacts between the α_2 - β_4 loop and another molecule in the crystal lattice. Together, these data indicate that for Pof8 RRM2, the α_2 - β_4 loop is flexible in

solution and helix $\alpha 3$ appears to exist in two conformations: a major species where helix $\alpha 3$ is positioned on the β -sheet as in the crystal structure and a second minor species that may have alternate or unstable positioning of helix $\alpha 3$ relative to the β -sheet.

Discussion

Structural comparison of Pof8 with LARP7 xRRMs

The combination of helix $\alpha 3$, that lies across the β -sheet and over where the absent RNP2 and RNP1 would be, and conserved RNP3 sequence on the Pof8 RRM2 is unique to the xRRM class of atypical RRM, and led us to hypothesize that the Pof8 RRM2 is an xRRM. The human genuine La protein also contains an atypical RRM2 that we previously predicted to be an xRRM [50]. Below we compare the conserved structural and RNA recognition features for the existing examples of defined xRRMs (p65 and hLarp7), Pof8 RRM2, and human La protein (hLa) RRM2.

Pof8, p65, hLarp7, and hLa RRM2 vary in the lengths of the loops between β strands and helices, presence or absence of a $\beta 4'$, length of helix $\alpha 3$, and number of residues following $\alpha 3$ (Fig. 4). For all, the beginning of helix $\alpha 3$ is enriched in acidic residues that face the β -sheet surface at $\beta 4$ and $\beta 1$, followed by aromatic and hydrophobic residues over $\beta 3$ and $\beta 2$, respectively (Figs. 1B, 4). Comparison of the three LARP7 RRM2 structures revealed that they have several interactions in common between the β -sheet and helix $\alpha 3$. First, there is a salt bridge between a conserved basic (K/R) residue in the middle of $\beta 1$ and an acidic residue in the first turn of helix $\alpha 3$, which is conserved in Pof8 (Fig. 4A,E) and p65 (Fig. 4B,F) but

not present in hLarp7 (Fig. 4C,G). Second, there is a hydrophobic patch between an I/L residue in $\beta 1$, an I/L residue in the $\beta 4$ - $\alpha 3$ loop, and conserved Y-W residues in the second turn of helix $\alpha 3$ (Fig. 4A-C,E-G). These hydrophobic contacts may stabilize the $\beta 4$ - $\alpha 3$ loop and help to orient helix $\alpha 3$ on the β -sheet. Third, there is a stacking interaction between a conserved hydrophobic/aromatic residue in $\beta 3$ with the conserved Y in the second turn of helix $\alpha 3$ (Figs. 2F, 4A-C,E-G). The contacts from $\beta 1$ and $\beta 3$ with residues on the first two turns of helix $\alpha 3$ anchor it on the β -sheet. Interestingly, the conserved residues in $\beta 1$ and $\beta 3$ that interact with helix $\alpha 3$ are located in the positions of RNP2 and RNP1, respectively, in the canonical RRM (Fig. 1C) [52,53]. It appears that while the xRRM lacks RNP1 and RNP2 sequences that interact with RNA, these sites on the β -sheet have adapted to interact with and stabilize helix $\alpha 3$ on the β -sheet surface.

RNA-binding determinants of the xRRM

Based on the sequence and structural similarity of Pof8 to p65 and hLarp7 xRRMs (Fig. 1B,C), comparison to structures of xRRM-RNA complexes [31,42], and effects of Pof8 amino acid substitutions and deletions on TER1 binding and abundance *in vivo* and telomere lengths [15,16], we propose a putative RNA-binding interface. Residues involved in RNA binding are shown as sticks on the ribbon model for p65 and hLarp7 (Fig. 5B, C) [31,42]. p65 and hLarp7 xRRMs share a conserved binding pocket formed by residues on the third and fourth turn of helix $\alpha 3$ and the $\beta 3$ - $\beta 2$ strands (Fig. 5G). The binding pocket recognizes 2 or 3 nts, respectively,

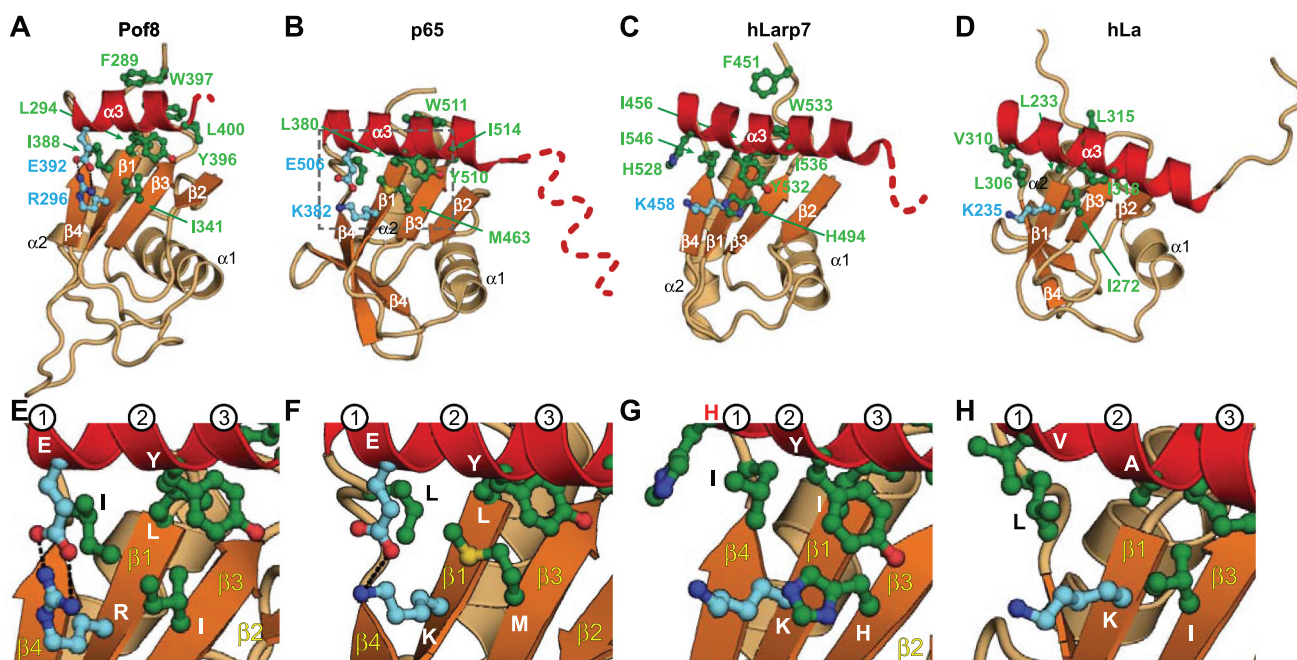


Figure 4. Comparison of structures of LARP7 xRRMs and hLa protein RRM2: helix $\alpha 3$ - β sheet interactions. Ribbon representations of RRM2 from (A) *S. pombe* Pof8, crystal structure (this work), (B) *Tetrahymena* p65, crystal structure (PDB ID 4EYT) and (C) human Larp7, solution NMR structure (PDB ID 5KNW), (D) human La, solution NMR structure (PDB ID 1OWX). Dashed line indicates disordered residues missing in the density and/or that become helical on binding RNA. (E-H) Zoomed regions of (A-D) highlighting the conserved residues important for $\alpha 3$ - β sheet interactions. The first three turns of helix $\alpha 3$ are numbered. Secondary structure motifs are coloured as in Fig. 2. Residue side chains important for $\alpha 3$ - β sheet interactions are shown as ball and stick and coloured green (hydrophobic) and cyan (charged).

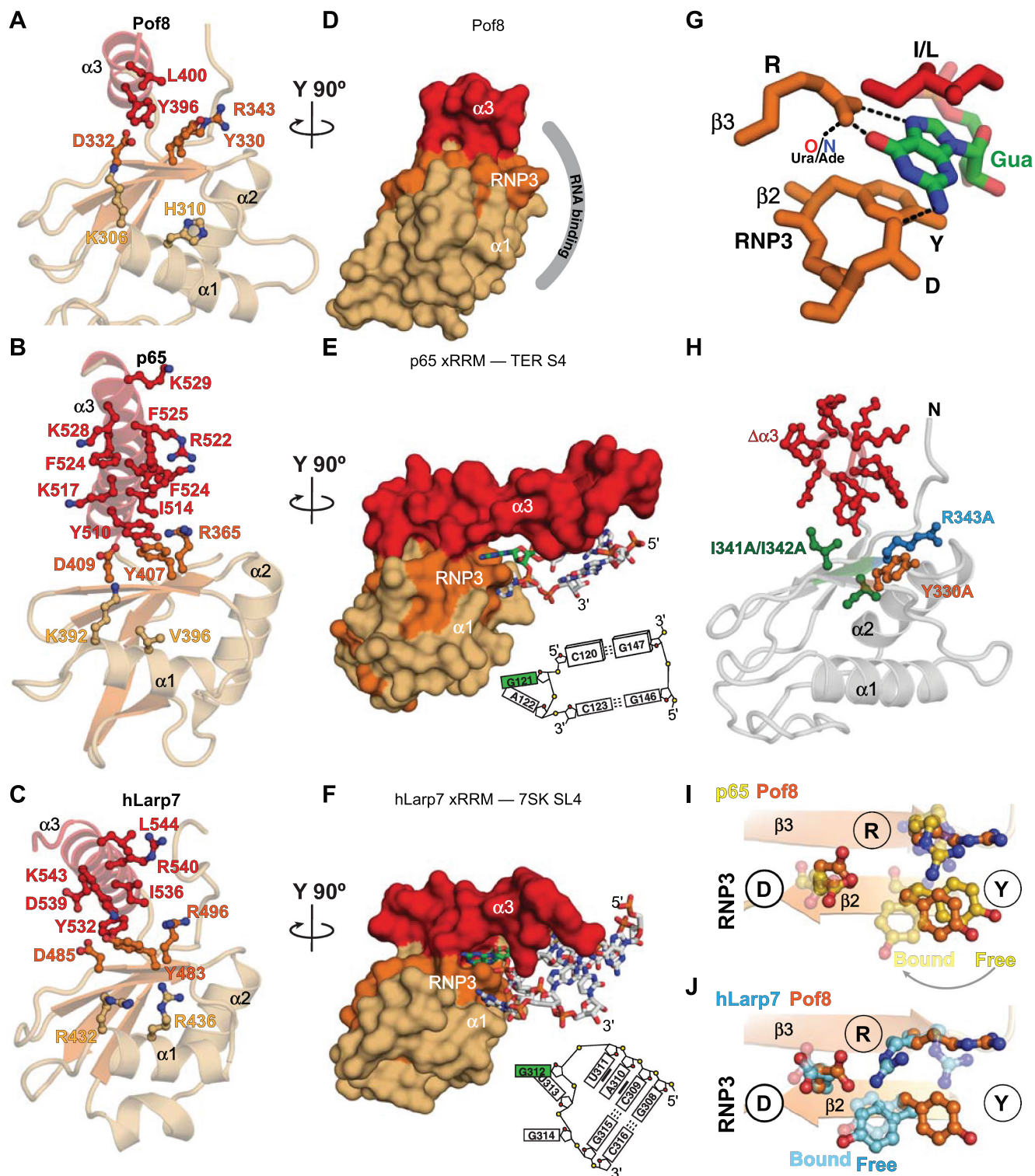


Figure 5. Comparison of structures of LARP7 xRRMs: RNA binding determinants (A–C) Ribbon representations of crystal structures of (A) Pof8 xRRM (this work), (B) p65 xRRM bound to telomerase RNA stem 4 (PDB ID 4ERD), (C) hLarp7 xRRM bound to 7SK stem-loop 4 (PDB ID 6D12). Side chains that interact (B, C) or are predicted to interact (A) with RNA are shown as sticks; (D–F) Surface representations of (D) Pof8 xRRM (this work), (E) p65 xRRM bound to telomerase RNA stem 4 (PDB ID 4ERD), (F) hLarp7 xRRM bound to 7SK stem-loop 4 (PDB ID 6D12), rotated 90° from (A–C). The proposed RNA interacting surface of Pof8 is shown by the grey arc, and for p65 and hLarp7 the interacting RNA nucleotides are shown as sticks, with Gua in green, and an RNA schematic is shown at right; (G) Stick representation of Gua recognition in the xRRM binding pocket. The interaction between $\beta 3$ R and a Ura O4 (e.g. hLarp7) or Ade N7 (e.g. p65) is also indicated; (H) Ribbon representation of Pof8 with residues whose substitution to alanine or deletion affect RNA binding *in vitro* or TER abundance and telomere length *in vivo* [15–17] shown as sticks. $\Delta\alpha 3$ is deletion of the entire helix. I341A/I342A is a double substitution. (I–J) Ribbon and stick representation illustrating position of RNP3 Y on (I) RNA free and bound p65 xRRM (gold) and RNA free Pof8 xRRM (orange) and (J) RNA free and bound hLarp7 xRRM (argon blue) and RNA free Pof8 xRRM (orange).

including one Gua, that insert into the binding pocket between helix $\alpha 3$ and $\beta 3$ – $\beta 2$ (Fig. 5E–G). The L on the third turn of helix $\alpha 3$ lies above the Gua, forming the ceiling of the

binding pocket (Fig. 5G). Pof8 RRM2 has a near-identical conserved binding pocket, including L on helix $\alpha 3$ turn 3 (Fig. 4A, Fig. 5A). The RNP3 Y–X–D sequence on $\beta 2$ and

R on $\beta 3$, previously identified as determinants of RNA binding [41], are identical among Pof8, p65, and hLarp7.

For p65 and hLarp7, the RNP3 and R on $\beta 3$ interact extensively with single-stranded RNA nucleotides, and alanine substitution of either Y ($\beta 2$, RNP3) or R ($\beta 3$) significantly impairs binding affinity to substrate RNA [31,42]. The conserved R on $\beta 3$ has two hydrogen bonds to the Hoogsteen edge of Gua while the conserved D on RNP3 hydrogen bonds to the Watson-Crick face. The Gua is further stabilized in the binding pocket by stacking interactions with helix $\alpha 3$ conserved I (I/L) above and conserved RNP3 Y residue below. The $\beta 3$ R also hydrogen bonds to AdeN7 (p65) or UraO4 (hLarp7) (Fig. 5G). In p65, the RNP3 Y undergoes a large change in position between the RNA-free and RNA-bound states (Fig. 5I), while in hLarp7 the position of RNP3 Y is already near to the bound state position prior to RNA binding (Fig. 5J). For the RNA-free Pof8 structure reported here, the position of RNP3 Y is close to that of free p65 (Fig. 5I).

In p65 and hLarp7, the longer helix $\alpha 3$ also binds to two or one base pairs, respectively. For p65, the long helix inserts between two stems on either side of the Gua-Ade bulge residues recognized in the binding pocket described above, causing a large bend between helices, while for hLarp7 a base pair at the top of the hairpin loop is recognized (Fig. 5E,F). We speculate that in Pof8, the two conserved lysines at the end of helix $\alpha 3$ might hydrogen bond to a base pair. Based on the above analysis, we conclude that Pof8 has a binding pocket for a Gua (or possibly a Ura) and at least one other nucleotide analogous to that for hLarp7 and p65.

Fig. 5H maps mutations and deletions that have been shown to affect Pof8 function *in vivo* [15–17] onto the crystal structure of Pof8. Deletion of helix $\alpha 3$ (residues 390–402) reduced TER1 levels in a similar manner as Pof8 deletion and caused telomere shortening [16], and I341A-I342A substitution, which would remove the hydrophobic contact between I341 ($\beta 3$) and Y396 ($\alpha 3$), also resulted in shortened telomeres, reduced TER1 levels, and reduced co-immunoprecipitation of Pof8 with TER1 [15]. These results indicate that helix $\alpha 3$ is essential for RNA binding and stability *in vivo* and are consistent with a requirement for stable positioning of helix $\alpha 3$ to form the RNA binding pocket. Single residue substitutions Y330A (RNP3) and R343A ($\beta 3$) had similarly deleterious effects *in vivo* compared to deletion of helix $\alpha 3$, deletion of the RRM, or full-length knock-down [16], consistent with their predicted importance for nucleotide recognition in the putative Pof8 RNA binding pocket (Fig. 5D).

Finally, we note that in Pof8, p65, hLarp7, and hLa, helix $\alpha 1$ contains a conserved basic (K/R) residue (Fig. 1B) that in hLarp7 interacts with RNA (Fig. 5F) [42]. A similar interaction may be present in the p65–RNA complex, but is not definitive since the sequence in this position in the crystal structure is not native [31]. We propose that this interaction is common to the LARP7 proteins, and may provide further RNA binding affinity and/or specificity. Based on our analysis of the structures, sequence, and mutagenesis data, we conclude that the Pof8 RRM2 is an xRRM, as discussed further below.

Comparison of LARP7 xRRMs to hLa RRM2

La protein generally binds RNA polymerase III transcripts after transcription, but does not remain associated with the RNA, in contrast to LARP7s. The hLa RRM2 has known chaperone activity and has broad RNA substrate recognition [2,10]. Compared to LARP7 RRM2s, hLa RRM2 has an extensive hydrophobic interface between helix $\alpha 3$ and the β -sheet, with the stacking and salt bridge interactions observed for LARP7 xRRMs absent (Fig. 4D,H). The hLa RRM2 helix $\alpha 3$ lies closer to the β -sheet and has an additional contact between $\beta 2$ and helix $\alpha 3$. hLa has an RNP3 (W261-I262-D263) characteristic of xRRMs, but the R on $\beta 3$ that is conserved among LARP7 xRRMs is replaced by an L (Figs. 1B, 4D). This R contributes to nucleotide specificity of LARP7 xRRMs through hydrogen bonding to bases, and its replacement in hLa protein with an L might explain the lower binding affinity and lack of specificity of hLa RRM2 vs LARP7 xRRMs [54,55]. As there are no structures to date of hLa RRM2 in complex with RNA, the binding mode is unknown. However, overall hLa RRM2 shares all essential features of an xRRM except for the conserved R ($\beta 3$). We propose that hLa RRM2 is an xRRM with reduced binding affinity in accordance with its function in binding multiple substrates.

A refined definition of xRRM

Pof8 and p65 are constitutive components of *S. pombe* and *Tetrahymena* telomerase, required for biogenesis and assembly of TER with TERT. The structure of Pof8 RRM2 reported here is the third example from the LARP7 family, and provides new insights into RNA binding by these domains and those of the related La proteins. The xRRM was first structurally characterized in p65 in the absence and presence of its cognate RNA [31], and subsequently in hLarp7 [42,50]. We note that the RRM2 of Larp7 and La protein have recently been alternatively designated as RRM2 α [2]; based on the work reported here we conclude that the xRRM and RRM α are the same RRM variant. Comparing the three LARP7 RRM2 structures shows that they share all the features of an xRRM first defined for p65 except for the strikingly variable length and sequence of helix $\alpha 3$ residues extending past the β -sheet (Fig. 4). Although in the absence of RNA the p65 helix $\alpha 3$ is a similar length to that of Pof8, upon RNA binding the helix is extended from four to eight turns (Fig. 4B). In free hLarp7 $\alpha 3$ has 5 turns and is extended by an additional turn on binding RNA. For both p65 and hLarp7 xRRMs, truncation of these extra turns of helix $\alpha 3$ resulted in significantly reduced binding affinity to substrate RNA [31,50], indicating that the region of helix $\alpha 3$ that extends beyond the β -sheet contributes to high affinity binding.

The sequence differences in helix $\alpha 3$ between p65 and hLarp7 appear to aid in substrate discrimination; the aromatic residues in p65 helix $\alpha 3$ insert orthogonal to the helical axis in the TER SL4 major groove to induce a sharp bend between the helices bracketing the GA bulge, while the basic residues in the hLarp7 helix $\alpha 3$ interact with and insert parallel to the major groove at the RNA apical loop [31,42]. The Pof8 helix $\alpha 3$ is three turns long and ends

at the protein C-terminus with two consecutive lysines, the last of which is disordered. It seems likely that the short Pof8 helix $\alpha 3$ will result in a weaker binding affinity compared to the xRRMs of p65 (30 nM) [31] and hLarp7 (100 nM) [42,50] to their cognate substrates. Additional affinity may be provided by interactions between conserved residues on helix $\alpha 1$ and RNA. In summary, this work has defined the structure of the recently discovered yeast telomerase holoenzyme protein Pof8 C-terminal domain and provided a more definitive description of the xRRM and its conserved versus variable determinants of RNA specificity and affinity.

Methods

Protein expression and purification

The gene encoding Pof8 RRM2 (residues 282–402) was codon optimized for *E. coli* and synthesized into a gBlock (Integrated DNA Technologies) and subsequently cloned into a pET-His₆-SUMO vector using Gibson ligation (New England Biolabs) [56]. The recombinant plasmid was subsequently transformed into *Escherichia coli* BL21 (DE3) cells (Agilent Technologies) for protein expression. Bacterial cultures were grown in LB media with 50 $\mu\text{g}/\text{ml}$ kanamycin at 37°C until OD₆₀₀ reached 0.6, then induced with a final concentration of 0.5 mM IPTG for 18–24 h at 18°C. Cells were harvested, sonicated in resuspension buffer (10% glycerol, 50 mM Tris pH 7.5, 750 mM NaCl, 30 mM imidazole, 3 mM NaN₃, 0.1% Triton-X 100, 1 mM 2-carboxyethyl phosphine (TCEP), sonicated and centrifuged at 17,000 rpm for 45 mins. Clarified cell lysate containing His₆-tagged protein was loaded onto a Ni-Sepharose affinity column (HisTrap HP; GE Healthcare). The column was washed with wash buffer (5% glycerol, 50 mM Tris pH 7.5, 750 mM NaCl, 30 mM imidazole, 3 mM NaN₃, 1 mM TCEP), then eluted with elution buffer (5% glycerol, 50 mM Tris pH 7.5, 750 mM NaCl, 300 mM imidazole, 3 mM NaN₃, 1 mM TCEP) to release bound His₆-SUMO-tagged Pof8 RRM2. The eluate was incubated with SUMO protease (expressed and purified in-house from a pET28a vector with an N-terminal His₆ tag) (approximately 0.5 mg protease to 5–10 mg Pof8 RRM2) for 3–4 hours at ambient temperature while dialysing against a buffer containing 20 mM Tris pH 7.5, 250 mM NaCl, 5 mM β -mercaptoethanol. The cleaved Pof8 RRM2 was purified by loading the cleavage reaction onto the Ni-Sepharose affinity column and collecting the flow-through. After further purification by size-exclusion chromatography (HiLoad 26/600 Superdex 75; GE Healthcare) in crystallization buffer (20 mM Tris, pH 7.5, 100 mM NaCl, 1 mM TCEP) or NMR buffer (20 mM NaPO₄ pH 6.1, 50 mM KCl, 1 mM TCEP), protein peak fractions were measured, pooled and concentrated using 3 KDa cut-off Amicon filters (Millipore Sigma). Unlabelled protein was purified from cells grown in LB media (Fisher Scientific) and uniformly ¹⁵N- or ¹⁵N,¹³C- labelled proteins were purified from cells grown in M9 minimal media with ¹⁵N ammonium chloride and/or ¹³C D-glucose (Cambridge Isotope Labs) as the sole nitrogen and/or carbon source, respectively.

NMR spectroscopy

NMR samples were concentrated to 0.1–0.8 mM in NMR buffer plus 5% D₂O. NMR experiments were performed at 298 K on AVANCE 800 MHz Bruker spectrometer equipped with HCN cryoprobe. Nearly complete backbone (N, H, C, Ca, C β , Ha, H β) assignments were obtained for all residues except residues in the $\alpha 2$ - $\beta 4$ loop (E361-L383), using standard triple resonance assignment experiments [57,58]. Briefly, 3D CBCACONH, HNCACB, HNCA, HBHACONH, HNCO and HNCACO experiments from the Bruker experimental suite were acquired on Topspin 4.0.7 (Bruker) using non-uniform sampling with 25% sparsity and a poisson-gap sampling schedule [59]. The experiments were processed with Topspin 4.0.7 and analysed using NMRFAM-SPARKY 1.414 [60] to assign backbone resonances [61,62]. After partial manual assignment, the I-PINE web server was used to validate assignments and obtain additional assignments for residues in the $\beta 1$ - $\alpha 1$ loop L300 and T304, $\alpha 1$ - $\beta 2$ loop E327, $\beta 2$ - $\beta 3$ loop K335-T338, $\beta 3$ - $\alpha 2$ loop K345, and $\alpha 2$ residue R358 [63]. The ¹⁵N- 3D NOESY experiment (noesyhsq-cetf3gp3d) from the Bruker experimental suite was acquired on Topspin 4.0.7 (Bruker) with a mixing time of 120 ms to obtain NOE crosspeaks to further validate assignments. For I-PINE, atomic coordinates from the crystal structure, pre-assignments from manually assigned resonances, and peak lists from ¹H-¹⁵N HSQC, ¹H-¹³C HSQC, HNCA, HNCACB, CBCACONH, CCONH, HBHACONH, HNCO, HNCACO, and ¹⁵N-NOESY spectra were included as input. The ¹H-¹⁵N heteronuclear NOE experiment (hsqnoef3gpsi) from the Bruker experimental suite was acquired on Topspin 4.0.7 (Bruker), processed with NMRPipe [64], analysed with NMRFAM-SPARKY 1.414 [60] and Office Excel (Microsoft), and plotted using matplotlib. The ¹⁵N T₁ (hsqct1etf3gpsi3d) and T₂ spin relaxation experiments (hsqct2etf3gpsi3d) from the Bruker experimental suite were acquired on Topspin 4.0.7 (Bruker), with interscan delays of 2.5 s and 3 s for T₁ and T₂ experiments, respectively. For T₁, the relaxation delays used were: 20 ms (in duplicate), 60 ms, 200 ms, 400 ms (in duplicate), 600 ms, 800 ms, and 1 s (in duplicate). For T₂, the relaxation delays were: 17 ms (in duplicate), 33.9 ms, 67.8 ms, 199 ms (in duplicate), 204 ms, 237 ms, and 271 ms (in duplicate). Data was processed with Topspin 4.0.7 and analysed with NMRFAM-SPARKY 1.414 and Office Excel (Microsoft). The measured T₁ and T₂ values were converted to R₁ and R₂ values and used to compute relative order parameters [51] using the equation $S^2 = (2R_2 - R_1)$. Relative order parameters (S^2_{rel}) were normalized to residue A340, located on $\beta 3$ in the hydrophobic core.

Crystallization and data processing

The 2D ¹H-¹⁵N HSQC of the Pof8 backbone amide resonances showed well-dispersed peaks, indicating a folded protein. The protein was concentrated to 25 mg/ml and crystallized in the hanging drop vapour diffusion method with reservoir solution 14% PEG 3350, 0.1 M NaNO₃, 0.1 M Tris pH 8.5 and drops containing 1 μl of protein and 1 μl reservoir. Rod shaped crystals appeared in one day, were cryoprotected in reservoir solutions containing 35% PEG 3350 and flash frozen in liquid

nitrogen. The native crystals diffracted to 1.35 Å. Crystals were soaked in 0.1 mM 4-chloro-mercuric-benzene-sulphonate (PCMBs) for 3–5 hours to obtain heavy atom (Hg) based experimental phases. All datasets were collected remotely at the Advanced Photon Source at Argonne National Labs, beamline 24-ID-C on a DECTRIS PILATUS 6 M detector. The Matthews coefficient suggested that there was one molecule of Pof8 RRM2 in an asymmetric unit. XDS/XSCALE [65,66] was used to index, integrate and scale the data. Conservative resolution limits were applied based on I/σ , $CC_{1/2}$ and R_{sym} values at the highest resolution shell. SAD phasing was performed by SHELXC/D/E [67] and HKL2MAP [68]. Four Hg sites were identified by SHELXD. SHELXE was used to assign the handedness of the model, produce initial phases and solvent flattening. Phases were further improved with SHARP [69], and an initial model was generated with AUTOSHARP [70] and BUCCANEER [71]. Native crystal structure was solved by Molecular Replacement using the Hg-model. The model was initially refined using Phenix version 1.13.2998 [72] and Coot [73], with final refinement performed using PHENIX with TLS refinement [74].

Multiple sequence alignment

The protein sequence alignment was performed with MUSCLE v 3.8 (EMBL-EBI, <https://www.ebi.ac.uk/Tools/msa/muscle/>). Alignments are displayed and annotated using ESPript 3 (<http://esript.ibcp.fr/>) with residues coloured by residue similarity. p65 residues 418–460 (β 2– β 3 loop), which are not involved in RNA recognition, were omitted from the sequence alignment due to lack of sequence homology to other LARP7 xRRMs.

Disclosure of potential conflicts of interest

No potential conflict of interest was reported by the authors.

Highlights

- The structure of the *S. pombe* LARP7 Pof8 C-terminal domain is an xRRM.
- Ciliates, human, and fission yeast contain LARP7 proteins with xRRMs involved in telomerase biogenesis.

With three examples of xRRM structures, we refine the definition of xRRM.

Data availability

Atomic coordinates and structure factors have been deposited in the Protein Data Bank with the accession code 6TZN. NMR chemical shift assignments have been deposited in the BioMagnetic Resonance Bank with the accession code 50002. All other data generated or analyzed in this study are included in the published article or are available from the corresponding author upon reasonable request.

Acknowledgments

This work was supported by NSF grant MCB1517625 and NIH grant R35GM131901 to J.F. The authors acknowledge NMR equipment grants NIH S10OD016336 and S10OD025073 and DOE grant DE-FC0202ER63421 for partial support of NMR and X-ray core facilities.

The authors thank M. Capel, K. Rajashankar, N. Sukumar, F. Murphy, I. Kourinov and J. Schuermann of Northeastern Collaborative Access Team (NE-CAT) beamline ID-24 at the Advanced Photon Source (APS) of Argonne National Laboratory, which are supported by NIH grants P41 RR015301 and P41 GM103403. Use of the APS is supported by DOE under Contract DE-AC02-06CH11357. The authors thank Dr. Lukas Sušac for help in the early stages of this work.

Funding

This work was supported by the National Institutes of Health [R35GM131901]; National Science Foundation [MCB1517625]; National Institutes of Health [S10OD016336], [S10OD025073], [P41 RR015301], [P41 GM103403]; Department of Energy [DE-FC0202ER63421], [DE-AC02-06CH11357].

Author Contributions

R.B. purified, crystallized, solved and analyzed the crystal structure of Pof8 xRRM; C.D.E. collected and analyzed NMR data and the structure; R.C. cloned, expressed, and purified Pof8 xRRM and collected NMR data; R.P. collected and analyzed NMR data; J.F. analyzed the structure and supervised the project; R.B., C.D.E., and J.F. wrote the manuscript; all authors edited the manuscript.

ORCID

Catherine D. Eichhorn  <http://orcid.org/0000-0001-8624-1961>

References

- [1] Bousquet-Antonelli C, Deragon JM. A comprehensive analysis of the La-motif protein superfamily. *RNA*. 2009;15:750–764.
- [2] Maraia RJ, Mattijssen S, Cruz-Gallardo I, et al. The La and related RNA-binding proteins (LARPs): structures, functions, and evolving perspectives. *Wiley Interdiscip Rev RNA*. 2017.
- [3] Bayfield MA, Yang R, Maraia RJ. Conserved and divergent features of the structure and function of La and La-related proteins (LARPs). *Biochim Biophys Acta*. 2010;1799:365–378.
- [4] Stefano JE. Purified lupus antigen La recognizes an oligouridylylate stretch common to the 3' termini of RNA polymerase III transcripts. *Cell*. 1984;36:145–154.
- [5] Puijn GJ, Slobbe RL, van Venrooij WJ. Analysis of protein–RNA interactions within Ro ribonucleoprotein complexes. *Nucleic Acids Res*. 1991;19:5173–5180.
- [6] Belisova A, Semrad K, Mayer O, et al. RNA chaperone activity of protein components of human Ro RNPs. *RNA*. 2005;11:1084–1094.
- [7] Teplova M, Yuan YR, Phan AT, et al. Structural basis for recognition and sequestration of UUU(OH) 3' termini of nascent RNA polymerase III transcripts by La, a rheumatic disease autoantigen. *Mol Cell*. 2006;21:75–85.
- [8] Vakiloroyaei A, Shah NS, Oeffinger M, et al. The RNA chaperone La promotes pre-tRNA maturation via indiscriminate binding of both native and misfolded targets. *Nucleic Acids Res*. 2017;45:11341–11355.
- [9] Bayfield MA, Vinayak J, Kerkhofs K, et al. La proteins couple use of sequence-specific and non-specific binding modes to engage RNA substrates. *RNA Biol*. 2019;1–10.
- [10] Blewett NH, Maraia RJ. La involvement in tRNA and other RNA processing events including differences among yeast and other eukaryotes. *Biochim Biophys Acta Gene Regul Mech*. 2018;1861:361–372.
- [11] Krueger BJ, Jeronimo C, Roy BB, et al. LARP7 is a stable component of the 7SK snRNP while P-TEFb, HEXIM1 and hnRNP A1 are reversibly associated. *Nucleic Acids Res*. 2008;36:2219–2229.

- [12] Markert A, Grimm M, Martinez J, et al. The La-related protein LARP7 is a component of the 7SK ribonucleoprotein and affects transcription of cellular and viral polymerase II genes. *EMBO Rep.* 2008;9:569–575.
- [13] Aigner S, Postberg J, Lipps HJ, et al. The Euplotes La motif protein p43 has properties of a telomerase-specific subunit. *Biochemistry.* 2003;42:5736–5747.
- [14] Witkin KL, Collins K. Holoenzyme proteins required for the physiological assembly and activity of telomerase. *Genes Dev.* 2004;18:1107–1118.
- [15] Collopy LC, Ware TL, Goncalves T, et al. LARP7 family proteins have conserved function in telomerase assembly. *Nat Commun.* 2018;9:557.
- [16] Mennie AK, Moser BA, Nakamura TM. LARP7-like protein Pof8 regulates telomerase assembly and poly(A)+TERRA expression in fission yeast. *Nat Commun.* 2018;9:586.
- [17] Paez-Moscoco DJ, Pan L, Sigauke RF, et al. Pof8 is a La-related protein and a constitutive component of telomerase in fission yeast. *Nat Commun.* 2018;9:587.
- [18] Nguyen VT, Kiss T, Michels AA, et al. 7SK small nuclear RNA binds to and inhibits the activity of CDK9/cyclin T complexes. *Nature.* 2001;414:322–325.
- [19] Yang Z, Zhu Q, Luo K, et al. The 7SK small nuclear RNA inhibits the CDK9/cyclin T1 kinase to control transcription. *Nature.* 2001;414:317–322.
- [20] Yazbeck AM, Tout KR, Stadler PF. Detailed secondary structure models of invertebrate 7SK RNAs. *RNA Biol.* 2018;15:158–164.
- [21] Marz M, Donath A, Verstraete N, et al. Evolution of 7SK RNA and its protein partners in metazoa. *Mol Biol Evol.* 2009;26:2821–2830.
- [22] He N, Jahchan NS, Hong E, et al. A La-related protein modulates 7SK snRNP integrity to suppress P-TEFb-dependent transcriptional elongation and tumorigenesis. *Mol Cell.* 2008;29:588–599.
- [23] Muniz L, Egloff S, Kiss T. RNA elements directing in vivo assembly of the 7SK/MePCE/Larp7 transcriptional regulatory snRNP. *Nucleic Acids Res.* 2013;41:4686–4698.
- [24] Greider CW, Blackburn EH. Identification of a specific telomere terminal transferase activity in Tetrahymena extracts. *Cell.* 1985;43:405–413.
- [25] Blackburn EH, Collins K. Telomerase: an RNP enzyme synthesizes DNA. *Cold Spring Harb Perspect Biol.* 2011.
- [26] Linger BR, Price CM. Conservation of telomere protein complexes: shuffling through evolution. *Crit Rev Biochem Mol.* 2009;44:434–446.
- [27] Lai AG, Pouchkina-Stantcheva N, Di Donfrancesco A, et al. The protein subunit of telomerase displays patterns of dynamic evolution and conservation across different metazoan taxa. *BMC Evol Biol.* 2017;17:107.
- [28] Chan H, Wang Y, Feigon J. Progress in human and tetrahymena telomerase structure determination. *Annu Rev Biophys.* 2017;46:199–225.
- [29] Wang Y, Feigon J. Structural biology of telomerase and its interaction at telomeres. *Curr Opin Struct Biol.* 2017;47:77–87.
- [30] Aigner S, Lingner J, Goodrich KJ, et al. Euplotes telomerase contains an La motif protein produced by apparent translational frameshifting. *Embo J.* 2000;19:6230–6239.
- [31] Singh M, Wang Z, Koo BK, et al. Structural basis for telomerase RNA recognition and RNP assembly by the holoenzyme La family protein p65. *Mol Cell.* 2012;47:16–26.
- [32] Akiyama BM, Loper J, Najjarro K, et al. The C-terminal domain of Tetrahymena thermophila telomerase holoenzyme protein p65 induces multiple structural changes in telomerase RNA. *RNA.* 2012;18:653–660.
- [33] Martino L, Pennell S, Kelly G, et al. Synergic interplay of the La motif, RRM1 and the interdomain linker of LARP6 in the recognition of collagen mRNA expands the RNA binding repertoire of the La module. *Nucleic Acids Res.* 2015;43:645–660.
- [34] Vinayak J, Marrella SA, Hussain RH, et al. Human La binds mRNAs through contacts to the poly(A) tail. *Nucleic Acids Res.* 2018;46:4228–4240.
- [35] Uchikawa E, Natchiar KS, Han X, et al. Structural insight into the mechanism of stabilization of the 7SK small nuclear RNA by LARP7. *Nucleic Acids Res.* 2015;43:3373–3388.
- [36] Jiang J, Miracco EJ, Hong K, et al. The architecture of Tetrahymena telomerase holoenzyme. *Nature.* 2013;496:187–192.
- [37] Egloff S, Van Herreweghe E, Kiss T. Regulation of polymerase II transcription by 7SK snRNA: two distinct RNA elements direct P-TEFb and HEXIM1 binding. *Mol Cell Biol.* 2006;26:630–642.
- [38] Nagai K, Oubridge C, Jessen TH, et al. Crystal structure of the RNA-binding domain of the U1 small nuclear ribonucleoprotein A. *Nature.* 1990;348:515–520.
- [39] Oubridge C, Ito N, Evans PR, et al. Crystal structure at 1.92 Å resolution of the RNA-binding domain of the U1A spliceosomal protein complexed with an RNA hairpin. *Nature.* 1994;372:432–438.
- [40] Maris C, Dominguez C, Allain FH. The RNA recognition motif, a plastic RNA-binding platform to regulate post-transcriptional gene expression. *FEBS J.* 2005;272:2118–2131.
- [41] Singh M, Choi CP, Feigon J. xRRM: a new class of RRM found in the telomerase La family protein p65. *RNA Biol.* 2013;10:353–359.
- [42] Eichhorn CD, Yang Y, Repeta L, et al. Structural basis for recognition of human 7SK long noncoding RNA by the La-related protein Larp7. *Proc Natl Acad Sci U S A.* 2018;115:E6457–E6466.
- [43] Aigner S, Cech TR. The Euplotes telomerase subunit p43 stimulates enzymatic activity and processivity in vitro. *RNA.* 2004;10:1108–1118.
- [44] Jacks A, Babon J, Kelly G, et al. Structure of the C-terminal domain of human La protein reveals a novel RNA recognition motif coupled to a helical nuclear retention element. *Structure.* 2003;11:833–843.
- [45] Ali N, Puijn GJ, Kenan DJ, et al. Human La antigen is required for the hepatitis C virus internal ribosome entry site-mediated translation. *J Biol Chem.* 2000;275:27531–27540.
- [46] Box JA, Bunch JT, Tang W, et al. Spliceosomal cleavage generates the 3' end of telomerase RNA. *Nature.* 2008;456:910–914.
- [47] Rubtsova MP, Vasilkova DP, Naraykina YV, et al. Peculiarities of Yeasts and Human Telomerase RNAs Processing. *Acta Naturae.* 2016;8:14–22.
- [48] Tang W, Kannan R, Blanchette M, et al. Telomerase RNA biogenesis involves sequential binding by Sm and Lsm complexes. *Nature.* 2012;484:260–264.
- [49] Holohan B, Kim W, Lai TP, et al. Impaired telomere maintenance in Alazami syndrome patients with LARP7 deficiency. *BMC Genomics.* 2016;17:749.
- [50] Eichhorn CD, Chug R, Feigon J. hLARP7 C-terminal domain contains an xRRM that binds the 3' hairpin of 7SK RNA. *Nucleic Acids Res.* 2016;44:9977–9989.
- [51] Lipari G, Szabo A. Model-free approach to the interpretation of nuclear magnetic resonance relaxation in macromolecules. 1. Theory and range of validity. *J Am Chem Soc.* 1982;104:4546–4559.
- [52] Martin-Tumasch S, Richie AC, Clos LJ 2nd, et al. A novel occluded RNA recognition motif in Prp24 unwinds the U6 RNA internal stem loop. *Nucleic Acids Res.* 2011;39:7837–7847.
- [53] Li H, Tong S, Li X, et al. Structural basis of pre-mRNA recognition by the human cleavage factor Im complex. *Cell Res.* 2011;21:1039–1051.
- [54] Martino L, Pennell S, Kelly G, et al. Analysis of the interaction with the hepatitis C virus mRNA reveals an alternative mode of RNA recognition by the human La protein. *Nucleic Acids Res.* 2012;40:1381–1394.
- [55] Brown KA, Sharifi S, Hussain R, et al. Distinct dynamic modes enable the engagement of dissimilar ligands in a promiscuous atypical RNA recognition motif. *Biochemistry.* 2016;55:7141–7150.
- [56] Gibson DG, Young L, Chuang RY, et al. Enzymatic assembly of DNA molecules up to several hundred kilobases. *Nat Methods.* 2009;6:343–U341.
- [57] Reid DG, MacLachlan LK, Edwards AJ, et al. Introduction to the NMR of proteins. *Methods Mol Biol.* 1997;60:1–28.

- [58] Cavanagh J. Protein NMR spectroscopy: principles and practice. 2nd ed. Amsterdam; Boston: Academic Press; 2007.
- [59] Hyberts SG, Takeuchi K, Wagner G. Poisson-gap sampling and forward maximum entropy reconstruction for enhancing the resolution and sensitivity of protein NMR data. *J Am Chem Soc*. 2010;132:2145–2147.
- [60] Lee W, Tonelli M, Markley JL. NRMFAM-SPARKY: enhanced software for biomolecular NMR spectroscopy. *Bioinformatics*. 2015;31:1325–1327.
- [61] Cavanagh J, Fairbrother WJ, Palmer AGI, et al. Protein NMR Spectroscopy. San Diego, CA: Academic Press; 1996.
- [62] Marion D. An introduction to biological NMR spectroscopy. *Mol Cell Proteomics*. 2013;12:3006–3025.
- [63] Lee W, Bahrami A, Dashti HT, et al. I-PINE web server: an integrative probabilistic NMR assignment system for proteins. *J Biomol NMR*. 2019;73:213–222.
- [64] Delaglio F, Grzesiek S, Vuister GW, et al. NMRPipe: a multidimensional spectral processing system based on UNIX pipes. *J Biomol NMR*. 1995;6:277–293.
- [65] Kabsch W. Integration, scaling, space-group assignment and post-refinement. *Acta Crystallogr D Biol Crystallogr*. 2010;66:133–144.
- [66] Kabsch W. Xds. *Acta Crystallogr D Biol Crystallogr*. 2010;66:125–132.
- [67] Sheldrick GM. Experimental phasing with SHELXC/D/E: combining chain tracing with density modification. *Acta Crystallogr D Biol Crystallogr*. 2010;66:479–485.
- [68] Pape T, Schneider TR. HKL2MAP: a graphical user interface for macromolecular phasing with SHELX programs. *J Appl Crystallogr*. 2004;37:843–844.
- [69] Bricogne G, Vonrhein C, Flensburg C, et al. Generation, representation and flow of phase information in structure determination: recent developments in and around SHARP 2.0. *Acta Crystallogr D Biol Crystallogr*. 2003;59:2023–2030.
- [70] Vonrhein C, Blanc E, Roversi P, et al. Automated structure solution with autoSHARP. *Methods Mol Biol*. 2007;364:215–230.
- [71] Cowtan K. The Buccaneer software for automated model building. 1. Tracing protein chains. *Acta Crystallogr D Biol Crystallogr*. 2006;62:1002–1011.
- [72] Adams PD, Afonine PV, Bunkoczi G, et al. PHENIX: a comprehensive Python-based system for macromolecular structure solution. *Acta Crystallogr D Biol Crystallogr*. 2010;66:213–221.
- [73] Emsley P, Cowtan K. Coot: model-building tools for molecular graphics. *Acta Crystallogr D Biol Crystallogr*. 2004;60:2126–2132.
- [74] Painter J, Merritt EA. Optimal description of a protein structure in terms of multiple groups undergoing TLS motion. *Acta Crystallogr D Biol Crystallogr*. 2006;62:439–450.